THE JOURNAL OF PHYSICAL CHEMISTRY B
A JOURNAL OF THE AMERICAN CHEMICAL SOCIETY

pubs.acs.org/JPCB

Article

Elucidating the pH Effects on Oleic Acid and Interactions with Lipid Membranes

Dongping Jiang, Yu-Chien Lin, Sungmin Shin, Younghwan Choe, and Nam-Joon Cho*

Cite This: J. Phys. Chem. B 2025, 129, 5976−5988

Read Online

ACCESS | Metrics & More | Article Recommendations | Supporting Information

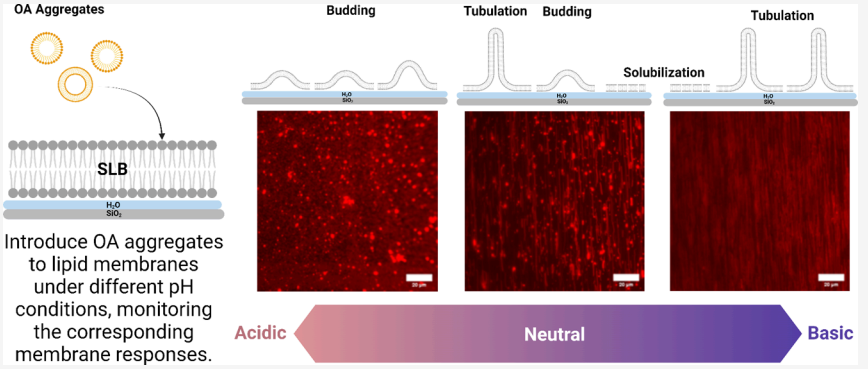

ABSTRACT: The interplay between fatty acids (FAs) and lipid membranes under varying pH conditions is important for deciphering fundamental cellular processes and advancing the design of responsive applications. Endowed with membrane incorporation, fatty acids (FAs) can induce curvature on membranes, resulting in alterations in fluidity, permeability, and stability. Despite the wide amount of research on membrane effects induced by FAs, the pH effect on their interaction behaviors remained unclear. Considering the varying pH environments in vivo, the study investigates how pH modulates the aggregation behavior of oleic acid (OA) and its subsequent interactions with lipid membranes. First, the critical aggregation concentration (CAC) was measured to determine the condition when aggregates formed. Less ordered aggregates with a lower zeta potential were observed under elevated pH conditions. These aggregates were further introduced to lipid membranes to evaluate the corresponding membrane responses using a QCM-D and fluorescence microscopy. pH shifts dramatically alter the OA protonation states of their headgroups, driving their insertion, orientation, and aggregation within membranes. Specifically, under lower pH levels, OA demonstrated an incorporation behavior into the membrane structure with increased membrane viscoelasticity, while disturbance of membrane structural integrity was observed under elevated pH levels. A transition from flatter budding protrusions to elongated tubes on the membrane was observed for incorporated OA, primarily owing to the increasing deprotonation degree that resulted in a change in the packing parameter. A stronger impact on cell viability at higher pH levels verified the membrane disruption behaviors. These findings elucidated that the protonation states of OA headgroups critically influence their membrane affinity and packing behavior, offering new perspectives for understanding membrane biophysics and designing pH-responsive delivery systems.

INTRODUCTION

Fatty acids (FAs) are fundamental molecules that serve as vital components of lipids[1] and play crucial roles in both health and disease including inflammation, vascular disorders, and cancer.[2−6] They also play a pivotal role as modulators of membrane properties and as participants in signal transduction pathways.[6−9] As amphiphilic molecules, FAs spontaneously self-assemble into aggregates in aqueous solutions, driven primarily by the hydrophobic interactions of their carbon tails.[10] Aggregation occurs when the concentration of FAs exceeds the critical aggregation concentration (CAC), at which point the attractive forces between hydrophobic chains outweigh the repulsion between the polar head groups to reach a thermodynamically favorable state.[11,12] Additionally, the aggregating behavior of FAs is highly sensitive to pH conditions, leading to the formation of diverse structures including micelles and vesicles.[13,14] FAs exhibit unique effects on membranes at concentrations above their critical aggregation concentration (CAC), where they induce membrane protrusions, disturbances, and remodeling.[15−19] These morphological changes primarily result from their incorporation into the membrane, which induces curvature stress on

Received: February 13, 2025
Revised: April 28, 2025
Accepted: May 5, 2025
Published: May 19, 2025

https://doi.org/10.1021/acs.jpcb.5c00994
J. Phys. Chem. B 2025, 129, 5976−5988

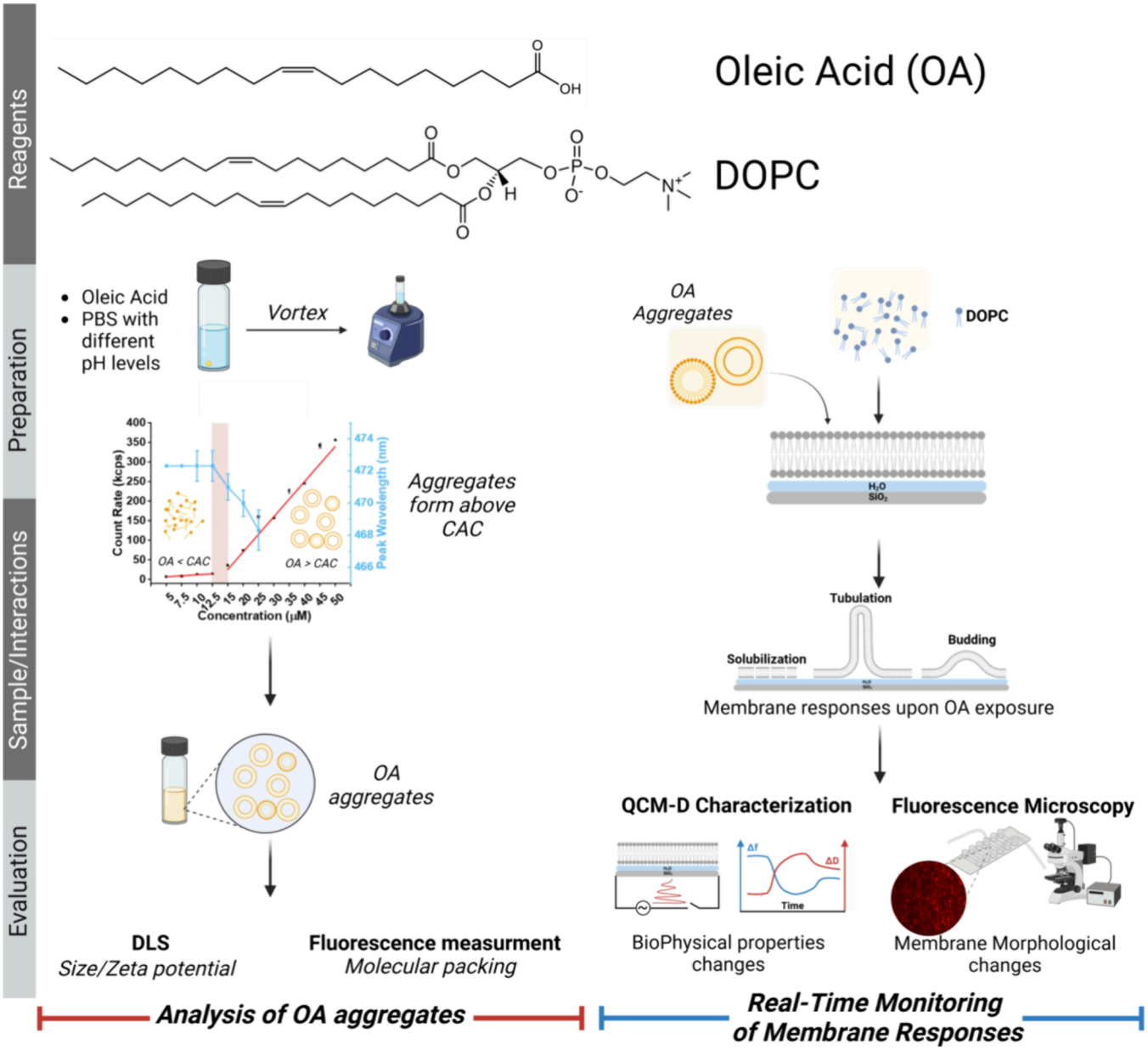

Figure 1. Schematic representation of experimental steps for investigations of membrane responses of oleic acid. Testing fatty acid solutions were prepared by dispersing oleic acid in a buffer followed by vortexing. OA aggregates formed above CAC values. The formed particles were then characterized by DLS and Laurdan fluorescence probes. The corresponding membrane interactions were monitored using QCM-D and fluorescence microscopy. CAC: critical aggregation concentration.

the surrounding lipids. Curvature stress refers to the mechanical tension arising from the geometric and compositional properties of the lipid molecules. Below the CAC, FAs exist as dispersed single molecules, leading to minimal membrane interaction.[17] Oleic acid (OA), a widely distributed FA with excellent biocompatibility,[20] is a major component of many membrane lipids that has been widely studied.[21] OA plays a critical role in modulating membrane structure, fluidity, and functionality.[19,22,23] It also undergoes dynamic aggregation behaviors above its CAC, transitioning in reverse between micelles to vesicles in response to pH variations driven by protonation states of OA molecules. The pK_a of the carboxyl group in solution is approximately 4.8, whereas in pure OA aggregates, it tends to be higher—around 8.[24] As the pH increases, deprotonation commences, resulting in a greater proportion of carboxylate headgroups. A deprotonated headgroup leads to an effective reduction in the packing parameter induced by increasing electrostatic repulsion between OA molecules.[25,26] A detailed understanding of how OA aggregates interact with lipid membrane under varying environmental conditions is therefore essential to both membrane biology and the development of responsive materials.[22,27,28]

Considering the different physiological pH levels, such as the small intestine (pH 7−8.5), skin (pH 4−5), and pancreas (pH ∼8.8),[29−31] the variations in pH environments have profound impacts on membrane properties, functions, and related biological processes.[32−36] Meantime, the local pH environment profoundly influences the behavior of OA in membranes. Variations in pH can alter the ionization state of FAs, leading to significant changes in their amphipathic character, packing

https://doi.org/10.1021/acs.jpcb.5c00994
J. Phys. Chem. B 2025, 129, 5976−5988

parameter, and subsequent interaction with surrounding lipids.[37−39] Investigating the membrane behavior of OA under pH 5 to 9 can mimic its interplay with cell membranes in varying tissues. Although the biophysical interactions between FAs and lipid membranes have been extensively studied, a comprehensive understanding of the role of pH in molecular-level mechanistic governing FA behavior within lipid membranes remains incomplete.

Previous studies have mainly focused on the membrane behavior of FAs using vesicle systems together with techniques such as microscopy, dynamic light scattering, surface force apparatus measurements, and thermal analyses to evaluate the membrane effects.[19,40−44] While these approaches provide valuable information on the treated membranes, the interplay between environmental pH and the membrane behavior by FA−lipid interactions is neglected, and these approaches have frequently been limited in their ability to resolve the real-time phenomena that occur at the interface of FAs and membranes.

To address this gap, this study aims to elucidate how pH governs OA protonation states, their aggregating behavior, and the corresponding membrane interactions. Supported lipid bilayers (SLBs), designed to replicate the essential structural characteristics of biological membranes, were employed as a model membrane.[45,46] Combined with surface-sensitive monitoring techniques, such as quartz crystal microbalance-dissipation (QCM-D) and time-lapse fluorescence microscopy, both the macroscopic and microscopic alterations in structure and dynamics of OA−membrane interplay induced by pH variations were captured (Figure 1). Our findings reveal that a higher pH environment resulted in higher CAC values with a lower molecular packing order of the aggregates. Subsequently, we conducted the QCM-D and microscopy to provide a detailed characterization of OA insertion, aggregation, and pH-dependent OA−membrane lipid interplay, which facilitates the investigation on alterations in membrane properties including viscoelasticity and curvature. Furthermore, the findings of biophysical models were verified on in vitro cells. This work identified a pH-triggered transition in OA−membrane interactions, offering a mechanistic basis for pH-dependent biological processes. pH-responsive systems are increasingly being explored in the design of delivery systems, yet rational design requires predictive models of pH-dependent FA-membrane behavior. Furthermore, the dysregulated FA metabolism underlie pathologies like nonalcoholic fatty liver disease (NAFLD), where cellular pH homeostasis is often compromised.[47] By bridging molecular-level insights with physiological phenomena, this work provides an understanding for targeting FA−membrane interactions in therapeutic contexts.

MATERIALS AND METHODS

Materials. 1,2-Di(9*Z*-octadecenoyl)-*sn*-glycero-3-phosphocholine (DOPC) and 1,2-dioleoyl-*sn*-glycero-3-phosphoethanolamine-*N*-(lissamine rhodamine B sulfonyl) (ammonium salt) (Rh-PE) were purchased from Avanti Polar Lipids, Inc. Oleic acid (OA) and 6-dodecanoyl-*N*,*N*-dimethyl-2-naphthylamine (Laurdan) were purchased from Sigma-Aldrich (St. Louis, MO). Phosphate-buffered saline (PBS) was purchased from Gibco (Carlsbad, CA). Milli-Q-treated water (>18 MΩ·cm) (Millipore, Billerica, MA) was used for all solution preparation steps. All other materials were purchased from Sigma-Aldrich (St. Louis, MO). All solutions were prepared using deionized water treated with a Milli-Q system (>18 MΩ·cm) (Millipore, Billerica, MA).

Preparation of the OA Solution. The OA ethanol stock solution was prepared by dissolving OA in ethanol to obtain a concentration of 50 mM/mL. Testing solutions of OA were prepared by diluting the stock solution in PBS with different pH values to achieve experimental concentrations. The diluted solution was then vortexed for 30 s to prepare the OA aggregates in the PBS buffer at different pH values. Pure OA was sealed and stored in a cabinet at −20 °C, and test solutions were freshly made on the day of the experiment. To prevent oxidation, OA was stored in the original package and used immediately upon opening.

Determination of the Critical Aggregation Concentration (CAC). *Fluorescence Spectroscopy.* A fluorescence probe, 1-pyrenecarboxaldehyde, was used to determine the CAC values. It was diluted in PBS, and the fluorescence emission spectrum of the probe was recorded ranging from 400 to 600 nm with excitation wavelength at 365.5 nm by a spectrophotometer (Tecan Spark, Tecan, Zurich, Switzerland). To prepare the testing solutions, a stock solution of the probe was first prepared at a final concentration of 10 mM in methanol. On the day of experiment, a certain amount of the stock solution was added into a 4 mL vial, and methanol was evaporated for 30 min. A fatty acid testing solution was then added and vortexed to obtain the probe-OA solution. Ten microliters of the probe stock solution was added in 990 μL of the OA solution to make the final concentration of the probe to be 0.1 μM. All measurements for each sample were scanned three times, and the results were averaged.

Light Intensity Scattering. Light intensity scattering (Brookhaven Instruments, Holtsville, NY) was used to determine the CMC values using the maximum incident mode. This mode provides remarkable sensitivity during the detection of particle intensity at low concentrations.[48] When concentrations were reached around the CMC, there is a quick increase in the intensity reading of scattered light due to the formation of particles. Sample solutions for DLS measurements were prepared from OA stock solutions with PBS dilution into expected concentrations. All measurements for each sample were scanned three times and averaged to check the reproducibility.

Characterizations of the OA Aggregates. The particle size and zeta potential of the OA solution were investigated using light intensity scattering and a zeta PALS analyzer (Brookhaven Instruments, Holtsville, NY). For size distribution analysis, a scattering angle of 90° was applied to measure the effective diameters. All data were measured three times and averaged to obtain results.

Laurdan Generalized Polarization Assay. To analyze the molecular packing conditions of the OA aggregates, the Laurdan generalized polarization (GP) index—$GP = (I_{435} - I_{490})/(I_{435} + I_{490})$—was applied to characterize the packing order of OA molecules, where I_{435} is the fluorescence intensity of Laurdan at 435 nm and I_{490} is the fluorescence intensity of Laurdan at 490 nm. Upon the preparation of OA solutions, 10 μM Laurdan was added to the solution and incubated for 1 h in the dark at room temperature. The emission fluorescent intensity was then measured and collected at wavelengths of 435 and 490 nm using a spectrophotometer (Tecan Spark, Tecan, Zurich, Switzerland).

SLB Formation. Lipids for membranes in this project were composed of DOPC lipid at a concentration of 0.5 mg/mL.

https://doi.org/10.1021/acs.jpcb.5c00994
J. Phys. Chem. B 2025, 129, 5976−5988

Similarly, 0.5 mol % of Rh-PE was added for a visible bilayer for fluorescence microscope monitoring. The supported lipid bilayer (SLB) was formed using a solvent-assisted lipid bilayer (SALB) method.[46] Lipid was dissolved in chloroform and then dried under a nitrogen gas flow to obtain a dried lipid film on the vial to remove the organic solvent. The dried lipid was then dissolved in isopropyl alcohol before each experiment. The lipid solution was introduced into the sensor chamber for 15 min followed by a solvent exchange with an aqueous buffer to form the SLB.

Quartz Crystal Microbalance with Dissipation (QCM-D) Experiments. To monitor the membrane responses under the exposure of fatty acid, QCM-D experiments were conducted using a Q-Sense E4 instrument (Q-Sense AB, Gothenburg, Sweden). The QCM-D technique measures the changes in the frequency (Δf) and energy dissipation (ΔD) of the oscillation of a piezoelectric quartz crystal sensor chip over time. The shifts in frequency and dissipation reflect the viscoelastic and mass properties of the supported bilayer on the chip.[49] The sensor chip had an intrinsic frequency of 5 MHz and a sputter-coated, 50 nm-thick layer of silicon dioxide (model no. QSX 303, Q-Sense AB). Before each experiment, the sensor chip was cleaned in the sequence of water and ethanol and dried by a nitrogen flow. The cleaned sensor was then treated with oxygen plasma treatment for 1 min using a plasma cleaner (model no. PDC-002, Harrick Plasma, Ithaca, NY). The bilayers that formed using the above-mentioned method can be verified according to our protocol.[50] After the formation of the bilayer, the testing compound solution was introduced at a constant flow rate of 50 μL/min. A buffer rinsing step was then conducted to complete the procedure. A peristaltic pump (Reglo Digital, Ismatec, Glattbrugg, Switzerland) was used to inject sample solutions and buffers into the measurement chamber during experiments. The experimental data were collected at the third (n = 3), fifth (n = 5), seventh (n = 7), and ninth (n = 9) overtones using the QSoft (Q-Sense AB) software package. In this study, the fifth (n = 5) overtone was used for the analysis of frequency and dissipation changes.

Fluorescence Microscopy. Fluorescence microscopy was conducted to provide visible monitoring of the morphological changes on the bilayer after the treatment of the compound. An Eclipse TI-U inverted optical microscope (Nikon, Japan) with a 60× magnification (NA = 1.49) oil-immersion objective lens (Nikon) was used to measure the images of the bilayer. The images were collected by an iXon 512 × 512 pixel EMCCD camera (Andor Technology, Northern Ireland) with 0.267 × 0.267 μM^2 pixel size. The bilayer was illuminated by a fiber-coupled mercury lamp (Intensilight C-HGFIE, Nikon) using a TRITC filter to light the 1,2-dioleoyl-*sn*-glycero-3-phosphoethanolamine-*N*-(lissamine rhodamine B sulfonyl) (ammonium salt) (Rh-PE). Similarly, 0.5 mol % of Rh-PE was incorporated with DOPC lipids to fabricate the SLB using a SALB method.[51] During the test period, the buffer and testing compound were introduced under a continuous flow rate of 50 μL/min. The fluorescence images of the bilayer were recorded every 5 s until no significant changes were observed. The starting point t = 0 s was defined as the time when testing compounds started to inject.

Fluorescence Recovery after Photobleaching (FRAP). FRAP measurements were employed to assess the lateral diffusivity of phospholipids within SLBs labeled with Rh-PE lipids under experimental conditions. Lateral diffusivity, which reflects membrane fluidity and corresponds to the viscosity of lipid membranes, is a critical parameter.[52] The influence of the pH on membrane fluidity should be systematically investigated to validate the quality of the formed membranes. To measure, the membrane was photobleached using a 532 nm, 100 mW laser (Klastech Laser Technologies, Dortmund, Germany) to create circular bleach spots applied for 5 s. Fluorescence micrographs were captured every 2 s over a period of 120 s to monitor fluorescence recovery at the bleached area. The lateral diffusion coefficients were then calculated from the FRAP data by using the Hankel transform method, as implemented in Matlab (MathWorks, USA). In short, a Hankel transformation can be applied to solve the recovery of fluorescently labeled molecules after photobleaching. The Fick's law is transformed to $f_i(k, t) = f_i(k,0)\exp(-4\pi^2 D_i k^2 t)$, where k is the defined spatial frequency and D_i is the diffusion coefficient for the ith component.[53]

In Vitro Cell Viability Assessment. The effect of OA on cell viability under varying pH conditions was assessed by measuring the dehydrogenase activity in mouse fibroblast cells (L-929, ATCC, USA) and human breast cancer cells (MCF7, CLS Cell Lines Service, Eppelheim, Germany). Cell viability was determined using a Cell Counting Kit-8 (CCK-8) (Dojindo Molecular Technologies, Rockville, MD). Both cell lines were cultured in Dulbecco's modified Eagle medium (DMEM) supplemented with 10% fetal bovine serum (Gibco) and 1% penicillin−streptomycin (Hyclone). They were maintained in a humidified incubator at 37 °C with 5% CO_2. L-929 and MCF7 cells were seeded at a density of 1×10^4 cells per well in 96-well tissue culture plates. After 24 h of incubation, the cells were washed and replenished with fresh media adjusted to different pH values. The pH of the experimental media was modified using hydrochloric acid (HCl) and potassium hydroxide (KOH) before coincubation with cells and samples. A blank group of cells that were incubated in media with different pH levels was conducted to measure the pH tolerance of the cells. The cells were then treated with OA solutions and incubated under the same conditions for an additional 24 h. Following treatment, a 10% CCK-8 solution was added to each well, and the plates were incubated for 2 h. Cell viability was quantified by measuring the absorbance at 450 nm using a microplate reader (Tecan Spark, Tecan, Zurich, Switzerland). All experiments were performed three times to ensure reproducibility.

RESULTS AND DISCUSSION

Determination of the Effects of pH on Critical Aggregating Concentration (CAC) Values. First, the CAC values of OA under varying pH conditions were determined to assess the influence of pH on its aggregation behavior. As single-chain lipids, OA induces disturbances in phospholipid membranes through aggregate formation.[54,55] Therefore, the CAC values under experimental pH conditions were investigated to confirm the formation of OA aggregates for subsequent studies. The CAC values were determined using fluorescence spectroscopy, a well-established technique reported in previous studies.[17,51,55] The fluorescence behavior of the probe (1-pyrenecarboxaldehyde) varies depending on its embedding state in solution or aggregates, resulting in shifts in the peak wavelength of the emission spectra.[56] Additionally, DLS was employed to verify the presence of detectable aggregates. A decrease in peak wavelength or an increase trend in the measured count rate is defined as indicative of the CAC concentrations. The measured CAC values are plotted in

https://doi.org/10.1021/acs.jpcb.5c00994
J. Phys. Chem. B 2025, 129, 5976−5988

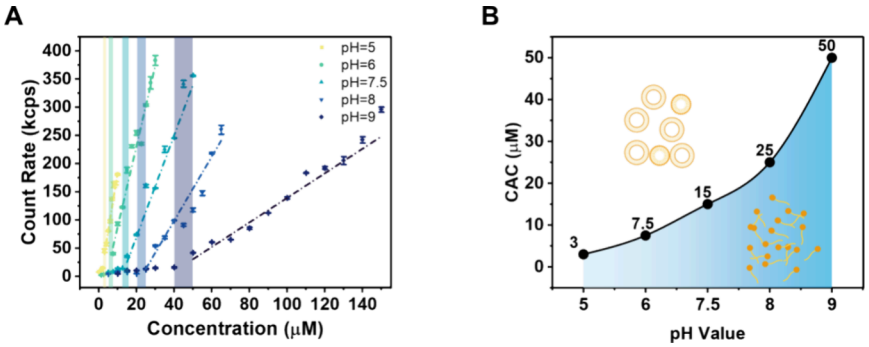

Figure 2. Determination of CAC values for OA under different pH environments. (A) The combined plots for light intensity scattering particle number measurements. The CAC values are defined as the kink point where an increase in the count rate begins. The vertical lines refer to the determined CAC values. (B) Summary of measured CAC values as a function of pH values, showing the increase in CAC values. OA aggregates form above the CAC values.

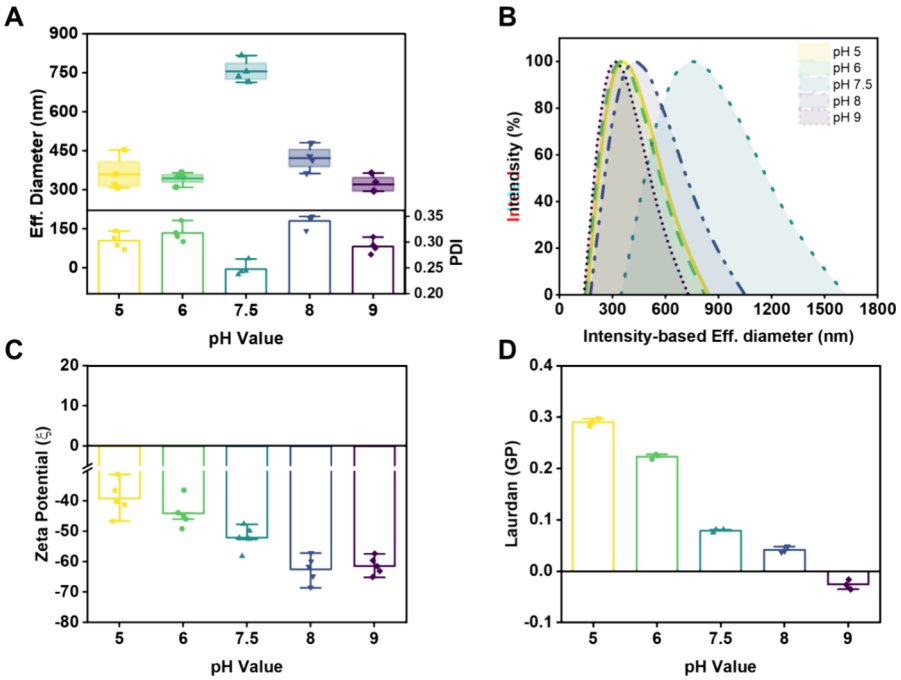

Figure 3. Characterizations of the OA aggregates. (A) The effective diameter of the OA aggregates in aqueous solutions under different pH values and intensity distribution of effective sizes. (B) Intensity-based size distributions of OA aggregates. (C) Corresponding zeta potentials (n = 3, mean ± SD). (D) The molecular packing order of oleic acid aggregations using the Laurdan generalized polarization index (Laurdan GP) of oleic acid solutions under varying pH values. Laurdan GP index = $(I_{440} - I_{490})/(I_{440} + I_{490})$, where 440 and 490 are the emission intensities at 440 and 490 nm, respectively. Laurdan was excited at 350 nm (n = 3, mean ± SD).

Figure S1. As shown in Figure 2A, where the CAC measurements (Figure S1) were collected, a clear increase in CAC values was observed as the pH increased. Below CAC, the count rate is comparable to that of the buffer solution, suggesting the absence of adequate aggregates in the solution. Upon the formation of aggregates, the measured CAC values increased from 3 μM at pH 5 to 50 μM at pH 9 (Figure 2B). Due to the improved deprotonation degree of OA as pH increased, the hydrophilicity of OA molecules is enhanced. The increased hydrophilicity strengthens the electrostatic repulsion between head groups and raises the thermodynamic barrier to stabilize the aggregates,[57−59] leading to higher CAC values.

Physical Properties of OA Aggregates. The characterizations of the OA aggregates have shown diverse aggregating behaviors under different pH values. The physical properties of these aggregates will be studied in this section. To ensure that, under the selected concentration, the aggregations were formed at an ideal condition based on the measured CAC values, a testing concentration of 200 μM/mL was selected as reported in previous studies.[16,18]

Size Distribution. The effective diameter of OA aggregates at a concentration of 200 μM was measured by DLS. Figure 3A illustrates the size distribution of the OA aggregates under various pH conditions. At lower pH values of pH 5 and 6, the measured diameter was 360.65 ± 57.08 and 343.87 ± 20.75 nm, respectively. Meanwhile, a notable increase in diameter at pH 7.5 was observed at 755.32 ± 38.28 nm, indicating that, under physiological pH conditions, partially deprotonated OA induced larger aggregating structures. When the environment pH value was further increased to 8 and 9, the size of the aggregations dropped to 421.95 ± 41.8 and 321.1 ± 28.8 nm. The observed decrease in size implies that in environments where the pH exceeds the pK_a, the enhanced number of

https://doi.org/10.1021/acs.jpcb.5c00994
J. Phys. Chem. B 2025, 129, 5976−5988

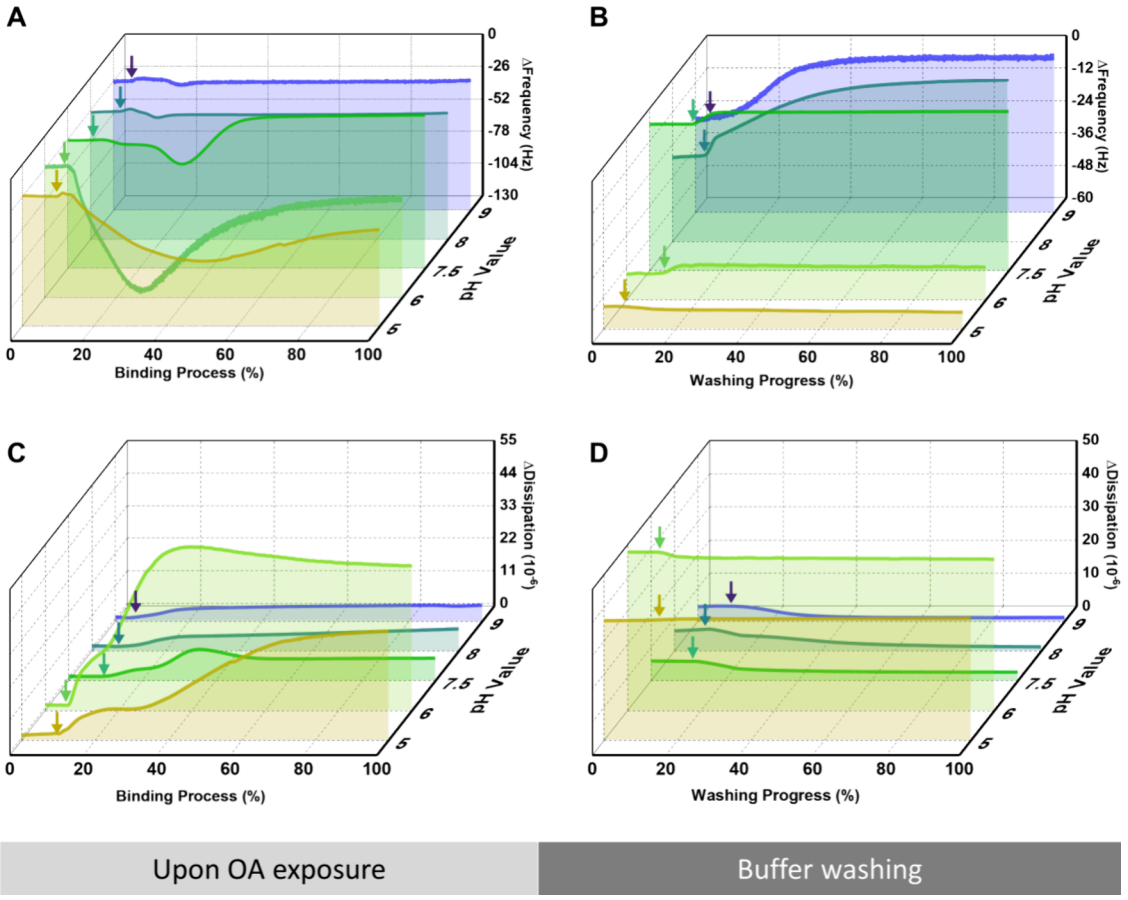

Figure 4. QCM-D curves of membrane responses treated with OA solution under different pH values for the fifth overtone. (A, C) The monitoring of Δf and ΔD plots as a function of time of the DOPC membrane under OA exposure for the whole binding process, respectively. Time was normalized by defining the moment when the OA solution was replaced for injection as 0% and the point at which the binding interactions end as 100%. (B, D) The representative Δf and ΔD responses during buffer washing. The washing time was normalized by setting the starting point of washing as 0% and the ending point as 100%. The arrows in panels A and C refer to the time point when OA reaches the bilayer, and those in panels B and D refer to the time point when the rinsing buffer enters the chamber.

charged headgroups decreases the packing parameter of OA molecules.[14,25] Meantime, the polydispersity indices (PDIs) of OA aggregates showed that the OA aggregates were not really evenly distributed, suggested by the PDI values around 0.3 for pH 5, 6, 8, and 9. The recorded PDI for pH 7.5 was slightly lower, indicating slightly lower size distributions owing to larger particle diameters. The intensity-based size distribution was collected from DLS shown in Figure 3B as a complementary data for the size distributions of the OA aggregates.

Zeta Potential. The zeta potential of prepared OA aggregates was measured and is presented in Figure 3C. There is a significant decrease in zeta potential observed from -39.16 ± 5.09 to -61.36 ± 2.68 mV as pH increased. Considering the pK_a of pure OA aggregates (pH ~8), more OA molecules will deprotonate as pH approaches pK_a, resulting in the decrease in zeta potential of OA aggregates.

Laurdan Generalized Polarization. To further understand the physical properties of these aggregations, a generalized polarization (GP) assay was performed by measuring the fluorescence emission of Laurdan incorporated into the OA aggregates, thereby allowing the detection of molecular packing order (Figure 3D).[60] The Laurdan GP value, calculated as $GP = (I_{435} - I_{490})/(I_{435} + I_{490})$, reflects the degree of lipid packing and membrane order, with higher GP values indicating a more tightly packed and ordered environment. The fluorescence behavior of Laurdan showed little dependence on pH conditions (Figure S2). As pH increased, the calculated Laurdan GP value dropped from 0.29 ± 0.006 to -0.026 ± 0.008 at pH 9. A higher Laurdan GP value indicates a denser lipid packing with a higher order.[61,62] Consequently, the degree of molecular packing order within OA aggregates decreased as pH increased owing to the increasing electrostatic repulsion force between OA molecules.[25]

The findings indicate the pH-dependent structural and biophysical properties of OA aggregates, including size distribution, zeta potential, and molecular packing order. Aggregates with less packing order and lower zeta potential were observed in an elevated pH environment.

Mass and Viscoelasticity Response Monitoring Induced by Oleic Acid under Different pH Values. A QCM-D monitoring was performed to investigate the corresponding effects on membranes induced by OA by collecting the real-time alterations in the changes of frequency (Δf) and energy dissipation (ΔD) signals. These measurements provided insights into the mass and viscoelastic properties of the membranes. A simplified membrane platform using 1,2-di(9Z-octadecenoyl)-*sn*-glycero-3-phosphocholine (DOPC) was prepared for experiments, which is widely used as a representative phospholipid of cell membranes.[17,63] To

https://doi.org/10.1021/acs.jpcb.5c00994
J. Phys. Chem. B 2025, 129, 5976−5988

avoid the interference of pH conditions on membranes, the properties of the membranes were investigated using fluorescence recovery after photobleaching (FRAP) analysis. The fluorescence intensity at the bleached area was almost fully recovered after 2 min (Figure S3A), indicating the intact lateral diffusion of the bilayer lipids. The calculated diffusion coefficients were 2.3 ± 0.2 μM^2 s^{-1} (Figure S3B) with an adequate mobile fraction of over 90%, in good agreement with the previously reported lateral diffusion of properly formed bilayers (Figure S3C).[64,65]

In this experiment, the prepared membrane was exposed to OA under a continuous flow rate of 50 μL/min followed by a buffer rinse. The arrows in the figures indicate the point at which the OA solution or buffer reached the bilayer chamber. The interactions between OA and the membrane are illustrated in Figure 4A,C. A decrease in Δf corresponds to an increase in the mass on the sensor, while an increase in ΔD signifies greater membrane instability and viscoelasticity. The viscoelasticity of the membrane can also be measured by monitoring Δf and ΔD at multiple overtones, where spread harmonic overtones indicate different osculation behaviors within the layer and higher viscoelasticity. The membrane was exposed to OA solution under appropriate pH conditions and followed by a washing process of the buffer.

Notably, when 200 μM OA solution under pH 5 reached the membrane chamber, the frequency (Δf) decreased gradually from −25.2 ± 0.1 to −77.6 ± 0.1 Hz (Figure 4A), signifying an increase in mass on the membrane system. Concurrently, dissipation (ΔD) signals increased slowly to 35.9 ± 0.1 × 10^{-6} Hz, reflecting enhanced membrane viscoelasticity. These signals stabilized at −53.9 ± 0.1 Hz (Δf) and 36.7 ± 0.1 × 10^{-6} Hz (ΔD), suggesting an increased viscoelasticity of the membrane (Figures 4B,D). The measured f−D relations showed a spread between different overtones, indicating increased viscoelasticity of the membranes (Figure S4).[18] A similar response was observed at pH 6, where the frequency changes (Δf) decreased more rapidly to −124.9 ± 0.2 Hz before stabilizing at −50.3 ± 0.1 Hz. The stronger dynamics and interactions between OA and the lipid membrane are primarily attributed to the enhanced ionic double layer surrounding OA aggregates due to the higher deprotonation degree. This formed ionic double layer enriched in positive charges exhibits stronger electrostatic interplays with the slightly negatively charged DOPC membranes.[66] Following buffer rinsing, no significant changes in Δf or ΔD were detected, indicating minimal membrane integrity disruption induced by OA incorporation. The f−D relations also possess substantial gaps between different overtones, suggesting an increased membrane viscoelasticity (Figure S4). These results demonstrate that under lower pH conditions, OA preferentially incorporates into the membrane, inducing lipid rearrangement and increasing membrane viscoelasticity.

Under pH 7.5, a distinct response was recorded. The frequency dropped steeply to −46.2 ± 0.2 Hz accompanied by a dissipation increase to 9.5 ± 0.1 × 10^{-6} Hz, indicating the attachment of OA aggregates to the membrane. Subsequently, the signals reversed and stabilized at −10.1 ± 0.3 Hz for Δf and 6.5 ± 0.1 × 10^{-6} Hz for ΔD. The increase in Δf to around −10 Hz indicated the removal of mass from the membrane. Exposure to OA at pH 7.5 rendered the membrane with lower viscoelasticity, as evidenced by reduced differences between different harmonic overtones (Figure S4). After buffer rinsing, Δf was further increased to around −7 Hz, indicating a further removal of membrane mass by disturbance from the incorporated OA. Meantime, ΔD significantly decreased to 2.5 ± 0.1 × 10^{-6} Hz, contrasting with values exceeding 30 × 10^{-6} Hz for membranes exposed to pH 5 and 6, indicating a more rigid system after treatment.

Membrane solubilization was observed under OA exposure at pH 8 and 9. At these pH levels, no significant decrease in Δf was observed, suggesting the removal of the membrane upon interaction. The high dissipation changes indicated membrane disturbance at the same time. The following buffer washing induced Δf increases to −0.6 ± 0.01 Hz (pH 8) and −2.4 ± 0.4 Hz (pH 9), while ΔD dropped to 1.2 ± 0.01 × 10^{-6} Hz (pH 8) and 1.0 ± 0.01 × 10^{-6} Hz (pH 9) (Figure 4). These changes reflect a significant mass loss that is consistent with membrane disruption and solubilization, as significant mass was removed from the sensor. The observed phenomenon is primarily attributed to increased curvature stress on the membrane induced by the incorporation of OA molecules.[67] At elevated pH levels, deprotonated OA exhibits a smaller packing parameter,[25] which induces higher curvature stress on the membrane. This stress leads to membrane destabilization, rupture, and disturbance, thereby damaging the structural integrity of the membrane.[68]

Membrane Response Observation under Oleic Acid Exposure. A time-lapse fluorescence microscope was applied to observe the real-time morphological changes on the membrane platform induced by OA aggregates (Figure 5).

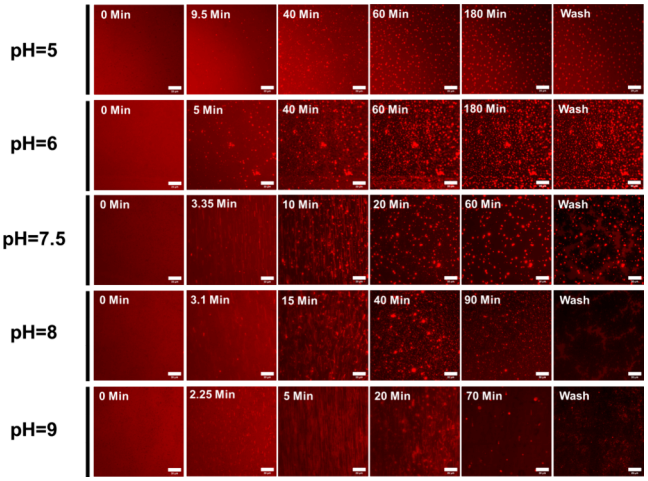

Figure 5. Fluorescent time-lapse microscopic images of the observation of membrane morphological responses induced by oleic acid under different pH values at a concentration of 200 μM. Representative snapshots of images depict the morphological changes at different time points. t = 0 min refers to the time point when oleic acid was changed for injection to the membrane channel. All scale bars are 20 μm.

To make the membrane visible under fluorescence, 0.5 mol % of Rh-PE was incorporated with DOPC. Following the formation of membranes, OA solutions were injected into the observation chamber, with t = 0 min marking the starting point of OA injection.

At lower pH values of 5 or 6, relatively flat undulations and protrusions were observed on the membrane surface, as evidenced by the formation of fluorescence-dense points. Under a top perspective, a budding-like protrusion will induce an area with higher density of fluorescent lipid as reported in

https://doi.org/10.1021/acs.jpcb.5c00994
J. Phys. Chem. B 2025, 129, 5976−5988

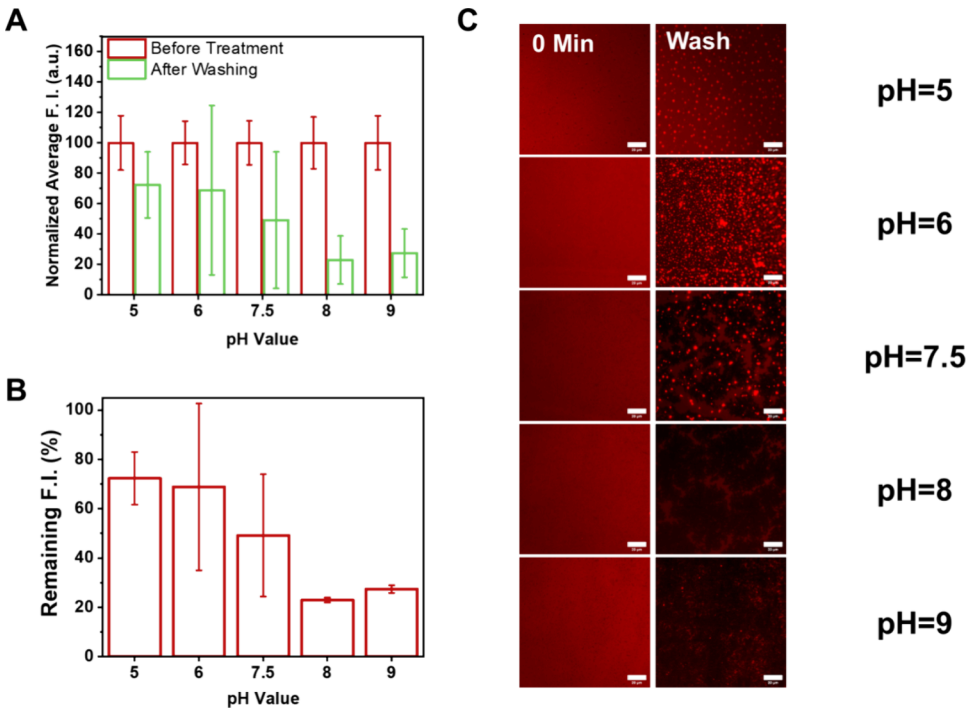

Figure 6. Normalized fluorescence intensity of the snapshots of fluorescence images observed before and after sample treatment and buffer rinsing. (A) Normalized average fluorescence intensity of the membranes before and after treatment. (B) Calculated remaining fluorescence intensity. (C) Corresponding snapshots of the images for intensity measurements under different pH values. All scale bars are 20 μm.

previous studies.[55] Approximately 5 min after OA injection, budding structures appeared under pH 6, while under pH 5, buddings first emerged at 9.5 min, aligning with QCM-D findings showing slower interaction dynamics at lower pH value. Under both conditions, the number of budding protrusions increased over time and stabilized upon further injection. Protrusions appeared more prominent under pH 6, as evidenced by the higher fluorescence from the membrane regions. Following PBS buffer rinsing, the budding structures remained intact, suggesting that the structural integrity of the membrane was not damaged.

At pH 7.5, close to physiological pH, both tubular and budding protrusions appeared on the membrane around 3.35 min after OA injection. The appearance of tubular protrusions is due to the increased deprotonation degree of OA, resulting in a greater difference between the packing parameters of OA and DOPC that induced a larger curvature stress surrounding the incorporated OA molecules.[69] As displayed in the snapshot image at 10 min after injection, elongated tubular and budding protrusions were observed on the membrane. After the elongated tubes were removed with continuous solution flow, budding-like protrusions were left on the membrane. After buffer rinsing, an uneven background fluorescence intensity was recorded, suggesting a partial membrane disruption caused by the incorporated OA.

When pH value increased to 8, more tubular protrusions were observed forming on the membrane from 3.1 min. Upon further rinsing, the observed budding structures deformed with twisting and elongating (Video S4), indicating a further increased curvature stress induced by incorporation of OA. Similar to what was observed under pH 7.5, the elongated structures were later transformed into buddings and then further decreased in intensity, indicating the continuous removal of membrane structures. Upon buffer rinsing, a significant decrease in fluorescence intensity was observed, indicating that the membrane disruption behavior correlated with the QCM-D observations.

A stronger membrane disrupting behavior was observed under a pH value of 9 where tubule structures were formed from 2.25 min after OA injection. The tubules were subsequently elongated during sample rinsing, indicating a bilayer solubilization behavior similar to the membrane interactions observed during SDS exposure.[63] The formed tubular structures were then removed, and a decrease in fluorescence intensity was observed upon treatment. Budding structures later appeared on the membrane that were elongated and rolled on the membrane (Video S5). The observation indicates the formation of DOPC-OA micelles due to higher lateral curvature stress that damages the structure of the membrane. After the buffer was washed, the detected fluorescence intensity was dramatically decreased, suggesting the disruption of the structural integrity of the membrane.

Taken together, the observed results showed a transformation in membrane responses as pH increases, which indicates the dynamic morphological effects of packing parameters of OA. Combined with the observations of membrane viscoelasticity from QCM-D, less membrane disturbance was observed under lower pH conditions, while under elevated pH conditions, a membrane disruption on structural integrity was observed.

To quantitatively investigate the membrane condition after OA exposure, the fluorescence intensity of the observed area of the membranes was investigated as shown in Figure 6. The measured intensity was normalized by setting the fluorescence intensity of 0 min for each condition at 100 au. The fluorescence intensity right after bilayer formation and after buffer rinsing was measured for comparison. After OA exposure under pH 5 and 6, the remaining intensity is 72.33

https://doi.org/10.1021/acs.jpcb.5c00994
J. Phys. Chem. B 2025, 129, 5976−5988

and 68.86% compared to their original intensity, indicating that although budding-like undulations were formed on the membrane, the structural integrity of the membrane remained. On the contrary, the fluorescence intensities of the treated membrane dropped significantly with only 22.9% left for pH 8 and 27.4% left for pH 9. This significant drop in intensity indicates damage to the structural integrity of the membrane under elevated pH conditions. The results verified the observed transformation of membrane morphological behavior from incorporation to disruption as the pH increases.

Dynamic Membrane Morphological Changes under Diverse pH Levels after Oleic Acid Incorporation. The morphological behaviors of incorporated OA were further studied by rinsing the OA-incorporated membrane with buffers at varying pH values. The pixel-intensity profiles of one selected protrusion were plotted at the end of the rinsing process (900 s) or at a certain point during rinsing (272.02 s under pH 8). The intensity plots provide insights into the morphological changes of structures formed on the membrane, which can alter the distribution and density of lipids including fluorescently labeled lipids. By evaluation of the fluorescence intensity of these morphological changes, their structural transformations can be monitored.

As shown in Figure 7, no significant morphology change was observed after washing with PBS buffer at pH 5, 6, and 7.5.

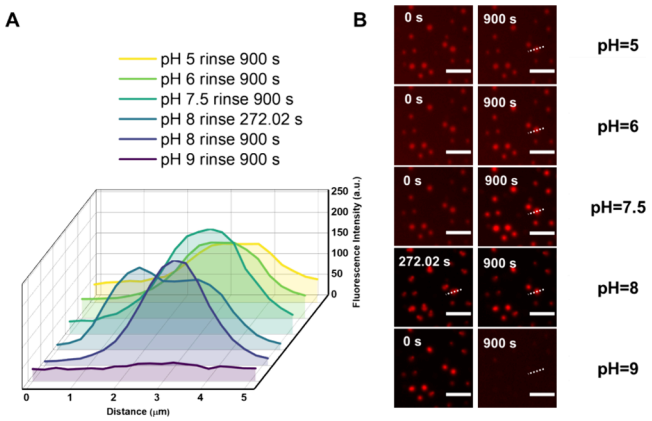

Figure 7. Evaluation of the morphology changes under different pH values after OA exposure. (A) The pixel intensity profile of one selected budding-like protrusion during the rinsing process to quantitatively analyze the intensity change. (B) Membrane morphology snapchats after OA exposure and rinsing with the PBS buffer from pH 5 to 9. The time on images refers to the time after the membrane was rinsed by the buffer under corresponding pH conditions. The white dash refers to the measuring path for intensity. All scale bars are 10 μm.

However, the peak intensity increased from 142.633 to 254.699 au, suggesting a higher density of fluorescent lipid. This increase in density indicates a growth in protrusion from the membrane surface. When the membrane was further rinsed by the buffer under pH 8, after approximately 272.02 s, elongated structures were observed growing from the buddings as evidenced by a shift in peak intensity point (see Figure 7B pH 8 at 272.02 s). The peak position was shifted from 2.97 to 1.89 μm, suggesting that the elongated structure has a length of 1.08 μm. Upon further rinsing, the elongated structure detached from the protrusions, as evidenced by changes in the peak position. When the environmental pH increased to 9, the peak disappeared, with the maximum fluorescence intensity reducing to 44.517 au, indicating the removal of the budding structures. Similarly, as the pH increased, more OA molecules became deprotonated, leading to a decrease in the OA packing parameter. This change created a larger disparity in packing parameters between DOPC and OA, resulting in higher curvature stress around the incorporated OA molecules. Consequently, a more pronounced disruption of the membrane was observed under elevated pH conditions.

The observation here supports the previous findings on the different interacting behaviors of OA when treated to membranes. Incorporated OA showed a similar transformation in membrane interaction behaviors from forming protrusions to membrane disruption as pH increases.

In Vitro Cell Viability Assessment. In addition to the observed membrane effects of OA at different pH values, its interactions with cell membranes were further investigated to corroborate the biophysical findings on model membranes. Healthy mouse fibroblast cells (L-929) and human breast cancer cells (MCF7) were exposed to OA under different pH environments with concentration gradient. First, the pH tolerance of L-929 and MCF7 was analyzed as depicted in Figure 8C,D (0 μM OA) where pH 7.5 was selected to be the control condition. No major effects on viabilities were observed among L-929 and MCF7 cultured within the range of pH 6 to 9, indicating that the relative alkaline or acidic environments were comparable to normal growing conditions. After 24 h incubation, both MCF-7 and L-929 cells present good resistance to the experimental testing pH conditions, and the pH is expected to be 5 with more than 90% viability. The concentration effects of OA on viabilities were then measured as shown in Figure 8A,B. Overall, the viability decreased as the OA concentration increased. When cocultured with L-929, no significant drop in viability was observed under pH 6 and 7.5 even under 400 μM/mL OA exposure. Meanwhile, under higher pH levels, the viability dropped quickly to around 70% when exposed to 25 μM/mL OA, indicating a potential disturbance on cell membranes. The cell viability fell to 33.56 $\pm$ 6.01% for pH 8 and 49.53 $\pm$ 4.28% for pH 9 under 400 μM/mL OA exposure. Similar trends were observed on MCF7 where the cell viability dropped significantly under elevated pH conditions. Notably, the effects of 200 μM/mL OA were compared to the control conditions as shown in Figure 8C,D to find correlations with biophysical findings. On L-929, there is a significant drop of viability from 100.65 $\pm$ 11.53 to 36.04 $\pm$ 5.03% under pH 8 and from 94.50 $\pm$ 16.06 to 49.39 $\pm$ 3.16% under pH 9. Compared to more than 80% viability under pH 6 and 7.5, the significant drop in viability indicates a stronger cytotoxicity on the cell potential due to the enhanced membrane disturbance. Similar results were found on MCF7 cell lines, where a significant drop in viability was observed under 200 μM/mL OA treatment. The summary of viabilities treated with 200 and 400 uM OA is listed in Table 1.

This significant difference in cell viability under different pH conditions indicates the potentially increased membrane disturbance at higher pH levels, reinforcing the biophysical findings that OA has a higher membrane disruption under elevated pH levels.

CONCLUSIONS

In summary, this study explored the dynamic interactions between OA aggregates and lipid membranes under different pH conditions, addressing a critical gap in understanding how environmental acidity governs the physicochemical dynamics

https://doi.org/10.1021/acs.jpcb.5c00994
J. Phys. Chem. B 2025, 129, 5976−5988

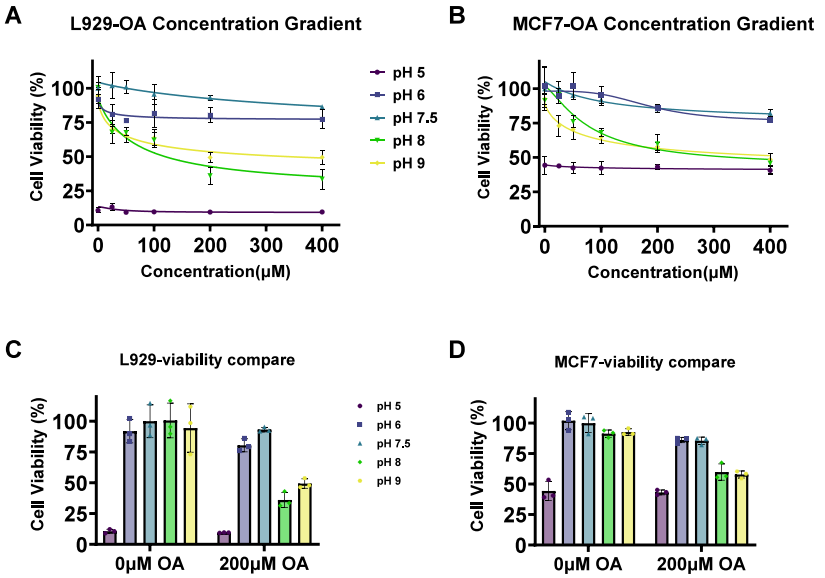

Figure 8. In vitro cell viability analysis on (A) mouse fibroblast cells (L-929) and (B) human breast cancer cells (MCF7) incubated with OA under different pH values. Cell viability of (C) L-929 and (D) MCF7 for the tolerance test under different pH levels and corresponding cell viabilities under 200 μM OA treatment (n = 3, mean ± SD). The graphs show the percentage of cell viability compared to the control group (cultured under pH 7.5) after 24 h of incubation.

Table 1. Summary of Cell Viability for L-929 and MCF-7 Treated with 200 and 400 uM OA under Different pH Levels

	L-929		MCF-7	
pH level	200 μM	400 μM	200 μM	400 μM
6	80 ± 4%	77 ± 6%	86 ± 2%	78 ± 2%
7.5	93 ± 2%	86 ± 1%	86 ± 2%	82 ± 3%
8	36 ± 5%	34 ± 6%	60 ± 5%	46 ± 6%
9	49 ± 3%	50 ± 4%	58 ± 2%	49 ± 3%

of amphiphilic biomolecules. Through a combination of QCM-D and time-lapse fluorescence microscopy, the real-time membrane responses of OA were elucidated, demonstrating pH-dependent behaviors from undulations and buddings to tubular protrusions and membrane solubilization. The changes in packing parameters induced by different degrees of deprotonation would significantly impact the interaction with membranes,[67] as a larger curvature stress was generated and induced stronger membrane disruptions under elevated pH conditions. As observed from the fluorescence microscope, budding-like protrusions were observed on the membrane under lower pH levels, while tubular protrusions, membrane solubilization, and damage on membrane integrity were observed at elevated pH levels. The observations from cell tests align with the findings on biophysical membranes, reinforcing the conclusion that the membrane interactions were relevant to the dynamic packing parameters of OA molecules under different protonation states. The findings highlight the vital role of pH as a regulator of FA−membrane lipid interactions, with broader implications for developing pH-stimulated delivery systems and biological processes such as membrane fusion and biological processes in non-neutral microenvironments like endosomes.

■ ASSOCIATED CONTENT

Supporting Information

The Supporting Information is available free of charge at https://pubs.acs.org/doi/10.1021/acs.jpcb.5c00994.

Measured critical aggregation concentration (CAC) for OA under different pH values; original QCM-D traces and frequency−dissipation relations at different overtones plotted from QCM-D curves for OA treatment on lipid membranes under corresponding pH values (PDF)

Fluorescence microscopy observations of DOPC lipid membranes containing 0.5 wt %Rho-PE lipid formed on glass surfaces under pH 5 (AVI)

Fluorescence microscopy observations of DOPC lipid membranes containing 0.5 wt %Rho-PE lipid formed on glass surfaces under pH 6 (AVI)

Fluorescence microscopy observations of DOPC lipid membranes containing 0.5 wt %Rho-PE lipid formed on glass surfaces under pH 7.5 (AVI)

Fluorescence microscopy observations of DOPC lipid membranes containing 0.5 wt %Rho-PE lipid formed on glass surfaces under pH 8 (AVI)

Fluorescence microscopy observations of DOPC lipid membranes containing 0.5 wt %Rho-PE lipid formed on glass surfaces under pH 9 (AVI)

Morphological monitoring of DOPC lipid membranes containing 0.5 wt % Rho-PE lipidformed on glass surfaces treated with OA at pH 5 (AVI)

■ AUTHOR INFORMATION

Corresponding Author

Nam-Joon Cho − *School of Materials Science and Engineering, Nanyang Technological University, 639798, Singapore; Centre for Cross Economy Global, Nanyang Technological University, 637551, Singapore; Singapore HUJ Alliance Research Enterprise (SHARE) 1 CREATE Way, Singapore-HUJ Alliance for Research and Enterprise, 138602,*

https://doi.org/10.1021/acs.jpcb.5c00994
J. Phys. Chem. B 2025, 129, 5976−5988

Singapore; orcid.org/0000-0002-8692-8955;
Email: njcho@ntu.edu.sg

Authors

Dongping Jiang − *School of Materials Science and Engineering, Nanyang Technological University, 639798, Singapore; Centre for Cross Economy Global, Nanyang Technological University, 637551, Singapore; Singapore HUJ Alliance Research Enterprise (SHARE) 1 CREATE Way, Singapore-HUJ Alliance for Research and Enterprise, 138602, Singapore*

Yu-Chien Lin − *School of Materials Science and Engineering, Nanyang Technological University, 639798, Singapore; Centre for Cross Economy Global, Nanyang Technological University, 637551, Singapore; Singapore HUJ Alliance Research Enterprise (SHARE) 1 CREATE Way, Singapore-HUJ Alliance for Research and Enterprise, 138602, Singapore;* orcid.org/0000-0003-3290-439X

Sungmin Shin − *School of Materials Science and Engineering, Nanyang Technological University, 639798, Singapore; Centre for Cross Economy Global, Nanyang Technological University, 637551, Singapore; Singapore HUJ Alliance Research Enterprise (SHARE) 1 CREATE Way, Singapore-HUJ Alliance for Research and Enterprise, 138602, Singapore*

Younghwan Choe − *School of Materials Science and Engineering, Nanyang Technological University, 639798, Singapore; Centre for Cross Economy Global, Nanyang Technological University, 637551, Singapore*

Complete contact information is available at: https://pubs.acs.org/10.1021/acs.jpcb.5c00994

Notes

The authors declare no competing financial interest.

■ ACKNOWLEDGMENTS

This work was supported by the Ministry of Education (MOE) in Singapore under grants RG111/20 and RG34/22. In addition, this research was also supported by the National Research Foundation, Singapore, through its Campus for Research Excellence and Technological Enterprise (CREATE) Project Code: 37018451. Figure [1,] was created with BioRender.com.

■ REFERENCES

(1) Karacor, K.; Cam, M. Effects of oleic acid. *Med. Sci. Discovery* **2015**, *2* (1), 125−132.
(2) Azevedo-Martins, A. K.; Monteiro, A. P.; Lima, C. L.; Lenzen, S.; Curi, R. Fatty acid-induced toxicity and neutral lipid accumulation in insulin-producing RINm5F cells. *Toxicology in Vitro* **2006**, *20* (7), 1106−1113.
(3) de Sousa Andrade, L. N.; Lima, T. M. d.; Curi, R.; Castrucci, A. M. d. L. Toxicity of fatty acids on murine and human melanoma cell lines. *Toxicology in Vitro* **2005**, *19* (4), 553−560.
(4) Rodriguez-Pacheco, F.; Gutierrez-Repiso, C.; Garcia-Serrano, S.; Alaminos-Castillo, M. A.; Ho-Plagaro, A.; Valdes, S.; Garcia-Arnes, J.; Gonzalo, M.; Andrade, R. J.; Moreno-Ruiz, F. J.; et al. The pro-/anti-inflammatory effects of different fatty acids on visceral adipocytes are partially mediated by GPR120. *European Journal of Nutrition* **2017**, *56* (4), 1743−1752.
(5) Nicolosi, R. J.; Woolfrey, B.; Wilson, T. A.; Scollin, P.; Handelman, G.; Fisher, R. Decreased aortic early atherosclerosis and associated risk factors in hypercholesterolemic hamsters fed a high- or mid-oleic acid oil compared to a high-linoleic acid oil. *Journal of Nutritional Biochemistry* **2004**, *15* (9), 540−547.
(6) De Carvalho, C. C. C. R.; Caramujo, M. J. The Various Roles of Fatty Acids. *Molecules* **2018**, *23* (10), 2583.
(7) Ibarguren, M.; López, D. J.; Escribá, P. V. The effect of natural and synthetic fatty acids on membrane structure, microdomain organization, cellular functions and human health. *Biochimica et Biophysica Acta (BBA)-Biomembranes* **2014**, *1838* (6), 1518−1528.
(8) Escribá, P. V.; Busquets, X.; Inokuchi, J.-i.; Balogh, G.; Török, Z.; Horváth, I.; Harwood, J. L.; Vígh, L. Membrane lipid therapy: Modulation of the cell membrane composition and structure as a molecular base for drug discovery and new disease treatment. *Prog. Lipid Res.* **2015**, *59*, 38−53.
(9) Gawrisch, K.; Soubias, O.; Mihailescu, M. Insights from biophysical studies on the role of polyunsaturated fatty acids for function of G-protein coupled membrane receptors. *Prostaglandins, Leukotrienes and Essential Fatty Acids* **2008**, *79* (3), 131−134.
(10) Maibaum, L.; Dinner, A. R.; Chandler, D. Micelle Formation and the Hydrophobic Effect. *J. Phys. Chem. B* **2004**, *108* (21), 6778−6781.
(11) Tanford, C. Theory of micelle formation in aqueous solutions. *J. Phys. Chem.* **1974**, *78* (24), 2469−2479.
(12) Fisicaro, E.; Compari, C.; Duce, E.; Biemmi, M.; Peroni, M.; Braibanti, A. Thermodynamics of micelle formation in water, hydrophobic processes and surfactant self-assemblies. *Phys. Chem. Chem. Phys.* **2008**, *10* (26), 3903−3914.
(13) Janke, J. J.; Bennett, W. F. D.; Tieleman, D. P. Oleic Acid Phase Behavior from Molecular Dynamics Simulations. *Langmuir* **2014**, *30* (35), 10661−10667.
(14) Morigaki, K.; Walde, P. Fatty acid vesicles. *Curr. Opin. Colloid Interface Sci.* **2007**, *12* (2), 75−80.
(15) Yoon, B. K.; Jackman, J. A.; Valle-González, E. R.; Cho, N.-J. Antibacterial Free Fatty Acids and Monoglycerides: Biological Activities, Experimental Testing, and Therapeutic Applications. *International Journal of Molecular Sciences* **2018**, *19* (4), 1114.
(16) Thid, D.; Benkoski, J. J.; Svedhem, S.; Kasemo, B.; Gold, J. DHA-Induced Changes of Supported Lipid Membrane Morphology. *Langmuir* **2007**, *23* (11), 5878−5881.
(17) Yoon, B. K.; Jackman, J. A.; Kim, M. C.; Sut, T. N.; Cho, N.-J. Correlating Membrane Morphological Responses with Micellar Aggregation Behavior of Capric Acid and Monocaprin. *Langmuir* **2017**, *33* (11), 2750−2759.
(18) Flynn, K. R.; Martin, L. L.; Ackland, M. L.; Torriero, A. A. J. Real-Time Quartz Crystal Microbalance Monitoring of Free Docosahexaenoic Acid Interactions with Supported Lipid Bilayers. *Langmuir* **2016**, *32* (45), 11717−11727.
(19) Kurniawan, J.; Suga, K.; Kuhl, T. L. Interaction forces and membrane charge tunability: Oleic acid containing membranes in different pH conditions. *Biochimica et Biophysica Acta (BBA) - Biomembranes* **2017**, *1859* (2), 211−217.
(20) Wang, Y.; Jiang, L.; Shen, Q.; Shen, J.; Han, Y.; Zhang, H. Investigation on the self-assembled behaviors of C18 unsaturated fatty acids in arginine aqueous solution. *RSC Adv.* **2017**, *7* (66), 41561−41572.
(21) Harayama, T.; Riezman, H. Understanding the diversity of membrane lipid composition. *Nat. Rev. Mol. Cell Biol.* **2018**, *19* (5), 281−296.
(22) Rath, E. M.; Duff, A. P.; Håkansson, A. P.; Vacher, C. S.; Liu, G. J.; Knott, R. B.; Church, W. B. Structure and Potential Cellular Targets of HAMLET-like Anti-Cancer Compounds made from Milk Components. *Journal of Pharmacy & Pharmaceutical Sciences* **2015**, *18* (4), 773−824.
(23) Muranushi, N.; Takagi, N.; Muranishi, S.; Sezaki, H. Effect of fatty acids and monoglycerides on permeability of lipid bilayer. *Chem. Phys. Lipids* **1981**, *28* (3), 269−279.
(24) Cistola, D. P.; Hamilton, J. A.; Jackson, D.; Small, D. M. Ionization and phase behavior of fatty acids in water: application of the Gibbs phase rule. *Biochemistry* **1988**, *27* (6), 1881−1888.

(25) Suga, K.; Kondo, D.; Otsuka, Y.; Okamoto, Y.; Umakoshi, H. Characterization of Aqueous Oleic Acid/Oleate Dispersions by Fluorescent Probes and Raman Spectroscopy. *Langmuir* **2016**, *32* (30), 7606−7612.
(26) Davis, J. G.; Zukowski, S. R.; Rankin, B. M.; Ben-Amotz, D. Influence of a Neighboring Charged Group on Hydrophobic Hydration Shell Structure. *J. Phys. Chem. B* **2015**, *119* (29), 9417−9422.
(27) Lyn, R. K.; Singaravelu, R.; Kargman, S.; O'Hara, S.; Chan, H.; Oballa, R.; Huang, Z.; Jones, D. M.; Ridsdale, A.; Russell, R. S.; et al. Stearoyl-CoA desaturase inhibition blocks formation of hepatitis C virus-induced specialized membranes. *Sci. Rep.* **2014**, *4* (1), 4549.
(28) Besada-Lombana, P. B.; Fernandez-Moya, R.; Fenster, J.; Da Silva, N. A. Engineering Saccharomyces cerevisiae fatty acid composition for increased tolerance to octanoic acid. *Biotechnol. Bioeng.* **2017**, *114* (7), 1531−1538.
(29) Gaohua, L.; Miao, X.; Dou, L. Crosstalk of physiological pH and chemical pKa under the umbrella of physiologically based pharmacokinetic modeling of drug absorption, distribution, metabolism, excretion, and toxicity. *Expert Opinion on Drug Metabolism & Toxicology* **2021**, *17* (9), 1103−1124.
(30) Duck, F. *Physical properties of tissues: a comprehensive reference book*; Academic Press: 2013.
(31) Valentin, J. Basic anatomical and physiological data for use in radiological protection: reference values: ICRP Publication 89. *Annals of the ICRP* **2002**, *32* (3−4), 1−277.
(32) Zhou, Y.; Raphael, R. M. Solution pH alters mechanical and electrical properties of phosphatidylcholine membranes: relation between interfacial electrostatics, intramembrane potential, and bending elasticity. *Biophys. J.* **2007**, *92* (7), 2451−2462.
(33) Aoi, W.; Marunaka, Y. Importance of pH Homeostasis in Metabolic Health and Diseases: Crucial Role of Membrane Proton Transport. *BioMed Res. Int.* **2014**, *2014* (1), No. 598986.
(34) Lengheden, A.; Jansson, L. pH effects on experimental wound healing of human fibroblasts in vitro. *European journal of oral sciences* **1995**, *103* (3), 148−155.
(35) Sim, P.; Song, Y.; Yang, G. N.; Cowin, A. J.; Garg, S. In Vitro Wound Healing Properties of Novel Acidic Treatment Regimen in Enhancing Metabolic Activity and Migration of Skin Cells. *International Journal of Molecular Sciences* **2022**, *23* (13), 7188.
(36) Kruse, C. R.; Singh, M.; Targosinski, S.; Sinha, I.; Sørensen, J. A.; Eriksson, E.; Nuutila, K. The effect of pH on cell viability, cell migration, cell proliferation, wound closure, and wound reepithelialization: In vitro and in vivo study. *Wound Repair Regener.* **2017**, *25* (2), 260−269.
(37) Xu, W.; Zhang, H.; Zhong, Y.; Jiang, L.; Xu, M.; Zhu, X.; Hao, J. Bilayers at High pH in the Fatty Acid Soap Systems and the Applications for the Formation of Foams and Emulsions. *J. Phys. Chem. B* **2015**, *119* (33), 10760−10767.
(38) Dowling, M. B.; Lee, J.-H.; Raghavan, S. R. pH-Responsive Jello: Gelatin Gels Containing Fatty Acid Vesicles. *Langmuir* **2009**, *25* (15), 8519−8525.
(39) Pashkovskaya, A. A.; Vazdar, M.; Zimmermann, L.; Jovanovic, O.; Pohl, P.; Pohl, E. E. Mechanism of Long-Chain Free Fatty Acid Protonation at the Membrane-Water Interface. *Biophys. J.* **2018**, *114* (9), 2142−2151.
(40) Lonchin, S.; Luisi, P. L.; Walde, P.; Robinson, B. H. A matrix effect in mixed phospholipid/fatty acid vesicle formation. *J. Phys. Chem. B* **1999**, *103* (49), 10910−10916.
(41) Chungcharoenwattana, S.; Ueno, M. Size control of mixed egg yolk phosphatidylcholine (EggPC)/oleate vesicles. *Chemical and pharmaceutical bulletin* **2004**, *52* (9), 1058−1062.
(42) Chungcharoenwattana, S.; Ueno, M. New vesicle formation upon oleate addition to preformed vesicles. *Chemical and pharmaceutical bulletin* **2005**, *53* (2), 260−262.
(43) BERGSSON, G.; ARNFINNSSON, J.; STEINGRÍMSSON, Ó.; THORMAR, H. Killing of Gram-positive cocci by fatty acids and monoglycerides Note. *Apmis* **2001**, *109* (10), 670−678.
(44) Shimokawa, N.; Mukai, R.; Nagata, M.; Takagi, M. Formation of modulated phases and domain rigidification in fatty acid-containing lipid membranes. *Phys. Chem. Chem. Phys.* **2017**, *19* (20), 13252−13263.
(45) Lee, T.-H.; Hirst, D. J.; Kulkarni, K.; Del Borgo, M. P.; Aguilar, M.-I. Exploring molecular-biomembrane interactions with surface plasmon resonance and dual polarization interferometry technology: expanding the spotlight onto biomembrane structure. *Chem. Rev.* **2018**, *118* (11), 5392−5487.
(46) Tae, H.; Yang, C.; Cho, N.-J. Artificial Cell Membrane Platforms by Solvent-Assisted Lipid Bilayer (SALB) Formation. *Accounts of Materials Research* **2022**, *3* (12), 1272−1284.
(47) Rainu, S. K.; Singh, N. Miniaturized Liver Disease Mimics to Gain Insights into MMP Expression during Disease Progression. *ACS Biomaterials Science & Engineering* **2025**, *11* (1), 476−484.
(48) Topel, Ö.; Çakır, B. A.; Budama, L.; Hoda, N. Determination of critical micelle concentration of polybutadiene-block-poly-(ethyleneoxide) diblock copolymer by fluorescence spectroscopy and dynamic light scattering. *J. Mol. Liq.* **2013**, *177*, 40−43.
(49) Rodahl, M.; Höök, F.; Krozer, A.; Brzezinski, P.; Kasemo, B. Quartz crystal microbalance setup for frequency and Q-factor measurements in gaseous and liquid environments. *Rev. Sci. Instrum.* **1995**, *66* (7), 3924−3930.
(50) Ferhan, A. R.; Yoon, B. K.; Park, S.; Sut, T. N.; Chin, H.; Park, J. H.; Jackman, J. A.; Cho, N.-J. Solvent-assisted preparation of supported lipid bilayers. *Nat. Protoc.* **2019**, *14* (7), 2091−2118.
(51) Shin, S.; Tae, H.; Park, S.; Cho, N.-J. Lipid Membrane Remodeling by the Micellar Aggregation of Long-Chain Unsaturated Fatty Acids for Sustainable Antimicrobial Strategies. *International Journal of Molecular Sciences* **2023**, *24* (11), 9639.
(52) Gohrbandt, M.; Lipski, A.; Grimshaw, J. W.; Buttress, J. A.; Baig, Z.; Herkenhoff, B.; Walter, S.; Kurre, R.; Deckers-Hebestreit, G.; Strahl, H. Low membrane fluidity triggers lipid phase separation and protein segregation in living bacteria. *EMBO J.* **2022**, *41* (5), No. e109800.
(53) Jönsson, P.; Jonsson, M. P.; Tegenfeldt, J. O.; Höök, F. A Method Improving the Accuracy of Fluorescence Recovery after Photobleaching Analysis. *Biophys. J.* **2008**, *95* (11), 5334−5348.
(54) Sun, C. Q.; O'Connor, C. J.; Roberton, A. M. Antibacterial actions of fatty acids and monoglycerides against Helicobacter pylori. *FEMS Immunology & Medical Microbiology* **2003**, *36* (1−2), 9−17.
(55) Yoon, B. K.; Jackman, J. A.; Park, S.; Mokrzecka, N.; Cho, N.-J. Characterizing the Membrane-Disruptive Behavior of Dodecylglycerol Using Supported Lipid Bilayers. *Langmuir* **2019**, *35* (9), 3568−3575.
(56) Goddard, E.; Turro, N.; Kuo, P.; Ananthapadmanabhan, K. Fluorescence probes for critical micelle concentration determination. *Langmuir* **1985**, *1* (3), 352−355.
(57) Small, D. M.; Cabral, D. J.; Cistola, D. P.; Parks, J. S.; Hamilton, J. A. The ionization behavior of fatty acids and bile acids in micelles and membranes. *Hepatology* **1984**, *4*, 77S−79S.
(58) Smith, A.; Lough, A. Micellar solubilization of fatty acids in aqueous media containing bile salts and phospholipids. *Br. J. Nutr.* **1976**, *35* (1), 77−87.
(59) Nagarajan, R.; Ruckenstein, E. Theory of surfactant self-assembly: a predictive molecular thermodynamic approach. *Langmuir* **1991**, *7* (12), 2934−2969.
(60) Harris, F. M.; Best, K. B.; Bell, J. D. Use of laurdan fluorescence intensity and polarization to distinguish between changes in membrane fluidity and phospholipid order. *Biochimica et Biophysica Acta (BBA) - Biomembranes* **2002**, *1565* (1), 123−128.
(61) Maitani, Y.; Nakamura, A.; Tanaka, T.; Aso, Y. Hydration of surfactant-modified and PEGylated cationic cholesterol-based liposomes and corresponding lipoplexes by monitoring a fluorescent probe and the dielectric relaxation time. *Int. J. Pharm.* **2012**, *427* (2), 372−378.
(62) Tae, H.; Park, S.; Tan, L. Y.; Yang, C.; Lee, Y.-A.; Choe, Y.; Wüstefeld, T.; Jung, S.; Cho, N.-J. Elucidating Structural Configuration of Lipid Assemblies for mRNA Delivery Systems. *ACS Nano* **2024**, *18* (17), 11284−11299.

https://doi.org/10.1021/acs.jpcb.5c00994
J. Phys. Chem. B 2025, 129, 5976−5988

(63) Yoon, B. K.; Jackman, J. A.; Kim, M. C.; Cho, N.-J. Spectrum of membrane morphological responses to antibacterial fatty acids and related surfactants. *Langmuir* **2015**, *31* (37), 10223−10232.
(64) Kim, M. C.; Gillissen, J. J. J.; Tabaei, S. R.; Zhdanov, V. P.; Cho, N.-J. Spatiotemporal dynamics of solvent-assisted lipid bilayer formation. *Phys. Chem. Chem. Phys.* **2015**, *17* (46), 31145−31151.
(65) Tabaei, S. R.; Choi, J.-H.; Haw Zan, G.; Zhdanov, V. P.; Cho, N.-J. Solvent-Assisted Lipid Bilayer Formation on Silicon Dioxide and Gold. *Langmuir* **2014**, *30* (34), 10363−10373.
(66) Zhang, X.; Yang, S. Nonspecific Adsorption of Charged Quantum Dots on Supported Zwitterionic Lipid Bilayers: Real-Time Monitoring by Quartz Crystal Microbalance with Dissipation. *Langmuir* **2011**, *27* (6), 2528−2535.
(67) Lowe, L. A.; Kindt, J. T.; Cranfield, C.; Cornell, B.; Macmillan, A.; Wang, A. Subtle changes in pH affect the packing and robustness of fatty acid bilayers. *Soft Matter* **2022**, *18* (18), 3498−3504.
(68) Akimov, S. A.; Volynsky, P. E.; Galimzyanov, T. R.; Kuzmin, P. I.; Pavlov, K. V.; Batishchev, O. V. Pore formation in lipid membrane II: Energy landscape under external stress. *Sci. Rep.* **2017**, *7* (1), 12509.
(69) Gontsarik, M.; Yaghmur, A.; Ren, Q.; Maniura-Weber, K.; Salentinig, S. From Structure to Function: pH-Switchable Antimicrobial Nano-Self-Assemblies. *ACS Appl. Mater. Interfaces* **2019**, *11* (3), 2821−2829.

https://doi.org/10.1021/acs.jpcb.5c00994
J. Phys. Chem. B 2025, 129, 5976−5988